NANO · MICRO small

www.small-journal.com

In Vivo mRNA CAR T Cell Engineering via Targeted Ionizable Lipid Nanoparticles with Extrahepatic Tropism

*Margaret M. Billingsley, Ningqiang Gong, Alvin J. Mukalel, Ajay S. Thatte, Rakan El-Mayta, Savan K. Patel, Ann E. Metzloff, Kelsey L. Swingle, Xuexiang Han, Lulu Xue, Alex G. Hamilton, Hannah C. Safford, Mohamad-Gabriel Alameh, Tyler E. Papp, Hamideh Parhiz, Drew Weissman, and Michael J. Mitchell**

With six therapies approved by the Food and Drug Association, chimeric antigen receptor (CAR) T cells have reshaped cancer immunotherapy. However, these therapies rely on ex vivo viral transduction to induce permanent CAR expression in T cells, which contributes to high production costs and long-term side effects. Thus, this work aims to develop an in vivo CAR T cell engineering platform to streamline production while using mRNA to induce transient, tunable CAR expression. Specifically, an ionizable lipid nanoparticle (LNP) is utilized as these platforms have demonstrated clinical success in nucleic acid delivery. Though LNPs often accumulate in the liver, the LNP platform used here achieves extrahepatic transfection with enhanced delivery to the spleen, and it is further modified via antibody conjugation (Ab-LNPs) to target pan-T cell markers. The in vivo evaluation of these Ab-LNPs confirms that targeting is necessary for potent T cell transfection. When using these Ab-LNPs for the delivery of CAR mRNA, antibody and dose-dependent CAR expression and cytokine release are observed along with B cell depletion of up to 90%. In all, this work conjugates antibodies to LNPs with extrahepatic tropism, evaluates pan-T cell markers, and develops Ab-LNPs capable of generating functional CAR T cells in vivo.

1. Introduction

Chimeric antigen receptor (CAR) T cell therapies have reshaped the cancer immunotherapy landscape, with six Food and Drug Administration (FDA)-approved CAR T cell immunotherapies for the treatment of relapsed or refractory acute lymphoblastic leukemia (ALL), B cell lymphomas, and multiple myeloma as well as additional cancer applications under investigation.[1–9] Currently, the production of these potent, autologous cell therapies relies on the complex process of ex vivo cell engineering. Briefly, harvested patient T cells are isolated, modified using viruses to express transmembrane CAR constructs, and reinfused into the patient. These CAR T cells then target and eliminate cancerous B cells, eradicating the cancer using the patient's own immune system.[10] However, because CAR expression is virally induced—thus, permanent and potent—these CAR T cells

M. M. Billingsley, N. Gong, A. J. Mukalel, A. S. Thatte, R. El-Mayta, S. K. Patel, A. E. Metzloff, K. L. Swingle, X. Han, L. Xue, A. G. Hamilton, H. C. Safford, M. J. Mitchell
Department of Bioengineering
University of Pennsylvania
Philadelphia, PA 19104, USA
E-mail: mjmitch@seas.upenn.edu

R. El-Mayta, M.-G. Alameh, T. E. Papp, H. Parhiz, D. Weissman
Department of Medicine
University of Pennsylvania
Philadelphia, PA 19104, USA

M.-G. Alameh, H. Parhiz, D. Weissman, M. J. Mitchell
Abramson Cancer Center
Perelman School of Medicine
University of Pennsylvania
Philadelphia, PA 19104, USA

The ORCID identification number(s) for the author(s) of this article can be found under https://doi.org/10.1002/smll.202304378

DOI: 10.1002/smll.202304378

M. J. Mitchell
Institute for Immunology
Perelman School of Medicine
University of Pennsylvania
Philadelphia, PA 19104, USA

M. J. Mitchell
Cardiovascular Institute
Perelman School of Medicine
University of Pennsylvania
Philadelphia, PA 19104, USA

M. J. Mitchell
Institute for Regenerative Medicine
Perelman School of Medicine
University of Pennsylvania
Philadelphia, PA 19104, USA

M. J. Mitchell
Penn Institute for RNA Innovation
Perelman School of Medicine
University of Pennsylvania
Philadelphia, PA 19104, USA

also attack healthy B cells after eliminating cancerous cells, leading to adverse effects such as cytokine release syndrome, long-term B cell aplasia, and pancytopenia, leaving patients at risk for severe infections.[5,11] Thus, there is a need for new approaches to engineer CAR T cells that provide potent cancer cell killing while mitigating the severity of these off-target effects.

mRNA-based cell engineering offers a number of advantages compared to viral transduction. From a production perspective, mRNA avoids concerns commonly associated with viral vectors such as limited cargo capacity, insertional mutagenesis, and in vivo immunogenicity.[12–15] Additionally, mRNA induces transient CAR expression, which mitigates the risks associated with long-term CAR T cell activity.[14–16] Specifically, this transient CAR expression allows for temporal control over CAR T cell therapy to prevent the prolonged presence of CAR T cells in the absence of cancer cells.[17,18] While this is advantageous in terms of safety, eliminating the long-term persistence associated with CAR T cells necessitates repeated dosing of the mRNA-based therapy.[16,19] In total, this potential has led to the evaluation of mRNA CAR T cell therapies in a variety of cancers including melanoma, Hodgkin's lymphoma, and ALL, which has demonstrated their ability to reduce short-term disease burden as effectively as viral engineered CAR T cells.[16,18,19] However, because mRNA degrades rapidly and does not readily cross the cell membrane, generating these mRNA CAR T cells requires optimized delivery methods.

One promising strategy for mRNA delivery is the use of nanoparticles as they can mitigate cytotoxicity, stabilize mRNA cargo, and enhance intracellular delivery.[20–23] Specifically, lipid nanoparticles (LNPs) have been utilized as platforms for potent mRNA delivery to a variety of cell types, as their ionizable lipid becomes charged in acidic environments to facilitate endosomal escape.[23–27] Further, their clinical applications have resulted in multiple FDA approvals including Alnylam's Onpattro siRNA LNP therapeutic and Moderna and Pfizer-BioNTech's COVID-19 mRNA LNP vaccines, making them a potentially ideal platform for mRNA delivery to other immune cells such as T cells.[28–30] In previous work, we have demonstrated potent T cell transfection using these LNPs and through excipient screening, established an optimized LNP platform for generating mRNA-based CAR T cells ex vivo.[31,32]

However, as the cost and complexity associated with ex vivo CAR T cell engineering can be prohibitive to its broad clinical implementation despite its therapeutic efficacy, there is a need to investigate alternative production strategies—such as the in vivo engineering of CAR T cells.[33–35] Delivering CAR mRNA to T cells in vivo—and thus, avoiding the process of leukapheresis and ex vivo T cell expansion—would streamline production and avoid the need for patient-specific manufacturing (**Figure 1**A). However, numerous obstacles complicate the transfection of T cells in vivo including the constant motility of circulating T cells that may decrease the duration of LNP-T cell interactions and the clearance of LNPs by the liver which may limit their bioavailability.[23,36,37] To overcome this first obstacle and improve LNP-T cell association, other nanoparticle platforms have utilized antibody conjugation to alter biodistribution, increase specificity to minimize off-target effects, and enhance delivery to target cell populations both in vitro and in vivo.[38–40] For T cell applications, many of these benefits have been demonstrated using polymeric NPs or LNPs targeted to various receptors[41] including CD3,[42,43] CD8,[43–45] CD4,[46–48] CD7,[49] CD5,[50] Nrp1,[51] and β_7.[40] However, there has not yet been an investigation directly comparing the efficacy of these various antibodies against different T cell markers to establish the best candidate for targeted mRNA delivery in vivo. Further, most antibody-based targeting strategies do not utilize nanoparticle platforms that have also been designed for delivery to tissues outside the liver. Thus, the targeted nanoparticle platforms are tasked with not only reaching the desired cell population but also overcoming hepatic accumulation. Here, the antibody conjugation targeting strategy was applied to a LNP platform that achieves extrahepatic transfection to aid in T cell targeting in vivo.

Thus, this work develops and evaluates antibody-functionalized LNP platforms (Ab-LNPs) for T cell targeting and demonstrates their potential for in vivo CAR T cell engineering. To generate Ab-LNPs, the previously established B10 LNP platform containing the C14-4 ionizable lipid was modified to include maleimide-functionalized PEG (mal-PEG) as previous work has validated this strategy for antibody-nanoparticle conjugation[43,44,47,48] (Figure 1B). Here, only antibodies against pan-T cell markers were investigated as excluding subpopulations of T cells—such as CD4+ or CD8+ T cells—may be detrimental to immunotherapy applications such as CAR T cell therapies.[52,53] Specifically, Ab-LNPs targeting the CD3, CD5, and CD7 pan T cell markers were formulated, and their functional delivery was compared to B10 LNPs[31,32] as well as the clinically relevant DLin-MC3-DMA LNPs[30,54] in vivo. Though many untargeted LNPs are reported to traffic primarily to the liver—thus demonstrating tropism counterproductive to the desired immune cell delivery[47,48,50]—all C14-4 LNPs demonstrated a bias for functional delivery in the spleen over the liver, and the Ab-LNPs demonstrated low levels of liver delivery indicative of their ability to bypass this organ and reach the target T cell population (Figure 1C).

The CD3 and CD7 Ab-LNPs were then explored for the in vivo delivery of therapeutic cargo—CD19 CAR-encoding mRNA. Both platforms yielded populations of circulating CAR T cells that significantly depleted the circulating B cell population, thus demonstrating their therapeutic potential for treating B cell cancers. Additionally, the cytokine levels in treated mice showed transient, dose-dependent elevations in the serum, supporting the potential of Ab-LNPs to aid in mitigating cytokine release and allow for repeat dosing. In all, three Ab-LNP platforms targeting pan-T cell markers were evaluated for T cell transfection, identifying CD3-LNPs and CD7-LNPs as delivery platforms capable of generating functional CAR T cells in vivo with dose-dependent influence over cytokine release, thus validating Ab-LNPs as a platform of in vivo CAR T cell production.

2. Results and Discussion

2.1. Designing and Screening a Library of T Cell Targeted Ab-LNPs In Vitro

Traditional LNP formulations include four components: i) an ionizable lipid to provide pH-dependent changes in charge that facilitate endosomal escape and potent intracellular delivery, ii) cholesterol for stability and membrane fusion, iii)

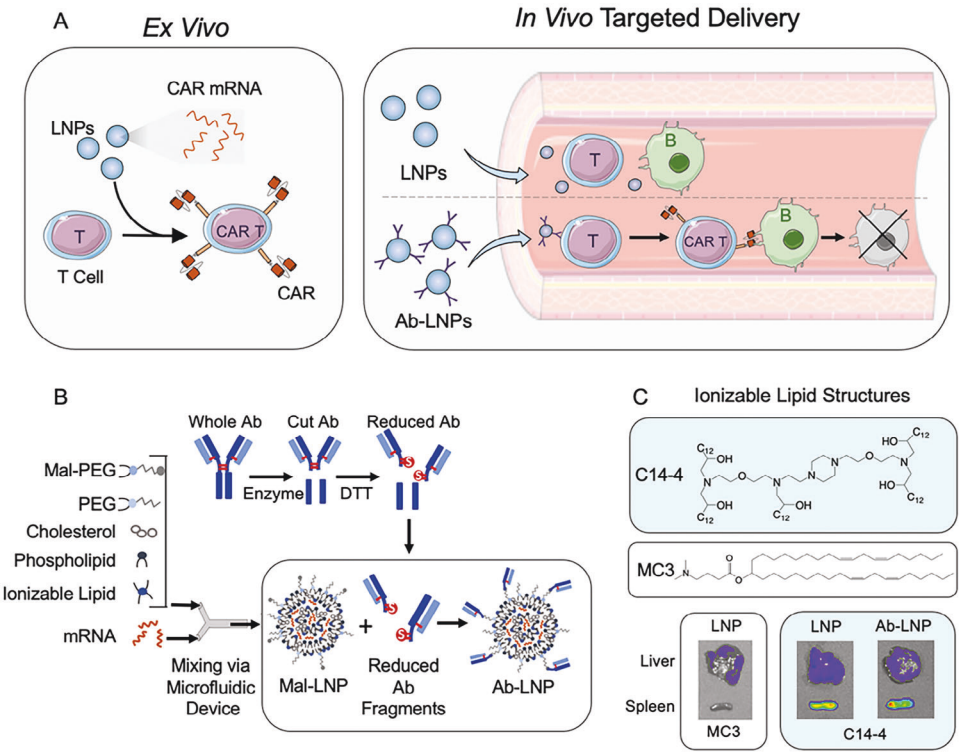

Figure 1. A) Schematic of the traditional and proposed CAR T cell engineering methods. In traditional LNP-based T cell transfection methods, the LNPs are combined with patient T cells ex vivo, generating CAR T cells outside of the body. In the proposed Ab-LNP-based T cell transfection, Ab-LNPs will be administered to the patient to generate the CAR T cell therapy in vivo, where antibodies facilitate T cell targeting. B) Schematic of Ab-LNP formation. An ethanol phase containing LNP components and an aqueous phase containing mRNA cargo are combined via microfluidic mixing to generate maleimide-functionalized LNPs (mal-LNPs) with maleimide-polyethylene glycol (mal-PEG) on their surface. These are combined with cut and reduced antibody fragments that conjugate to the mal-LNPs to form antibody-functionalized LNPs (Ab-LNPs). C) Structures of the clinical standard MC3 lipid and C14-4 ionizable lipid used to generate LNPs in this work and representative IVIS images of their respective performances in vivo demonstrating extrahepatic delivery using C14-4.

phospholipid for structural support and endosomal escape, and iv) lipid-anchored polyethylene glycol (PEG) to prevent aggregation and promote stability.[24,27,55,56] However, to generate antibody-functionalized LNPs (Ab-LNPs) for targeting applications, this traditional formulation was modified to include maleimide-functionalized lipid-anchored PEG (mal-PEG) as a fraction of the total PEG content. The addition of this maleimide to the surface of the LNP (mal-LNP) allows for binding of antibodies to the surface via thiol-maleimide interactions as demonstrated in previous work.[44,47] Thus, to generate antibody fragments capable of binding to the surface of the mal-LNPs, whole antibodies were cleaved to minimize size and remove the potentially inflammatory Fc region[57,58] and reduced (Figure 1B; Figure S1, Supporting Information). Specifically, IdeZ, Pepsin, and Ficin were used to separate the Fab and Fc regions of the antibodies targeting CD3, CD5, and CD7— representative pan-T cell antigens with durable expression—and the resulting fragments were then reduced using dithiothreitol (DTT) to reveal free thiols on the Fab fragments. These antibody fragments then bind to the mal-LNP surface to form Ab-LNPs, with any unconjugated antibody fragments—both Fc regions and unconjugated Fabs—removed using size exclusion chromatography.

To first determine the optimal amount of mal-PEG to incorporate, four mal-LNP formulations encapsulating luciferase-encoding mRNA were generated by holding the excipient molar ratios constant and varying only the ratio of mal-PEG to PEG, allowing for varied amounts of antibody to be conjugated to the mal-LNP surface (**Figure 2**A). The mal-LNPs were then conjugated with antibodies against human CD5, and their sizes were measured using dynamic light scattering (DLS) before and after this conjugation (Figure 2; Figure S2, Supporting Information). When compared to LNPs containing no mal-PEG (B10), the DLS measurements showed that all Ab-LNPs had a size increase while mal-LNPs did not significantly increase LNP diameter over B10. Thus, the increase in size observed for Ab-LNPs was attributed to antibody conjugation.

Using their size increase as evidence of successful conjugation, the Ab-LNPs were then screened for mRNA delivery and toxicity in Jurkat cells, a CD5+ human T cell line.[59–61] In this screen, luciferase-encoding mRNA was used as a model cargo as it requires intracellular delivery and translation to generate luciferase protein capable of interacting with luciferin reagent, thus allowing luminescent signal to serve as a measure of functional mRNA delivery. When quantifying this mRNA delivery as normalized to the standard B10 treatment group, Ab-LNPs were able to achieve as high as a 15-fold increase in luciferase mRNA delivery compared to B10 without significant toxicity (Figure 2B). All Ab-LNPs resulted in a significant increase in transfection

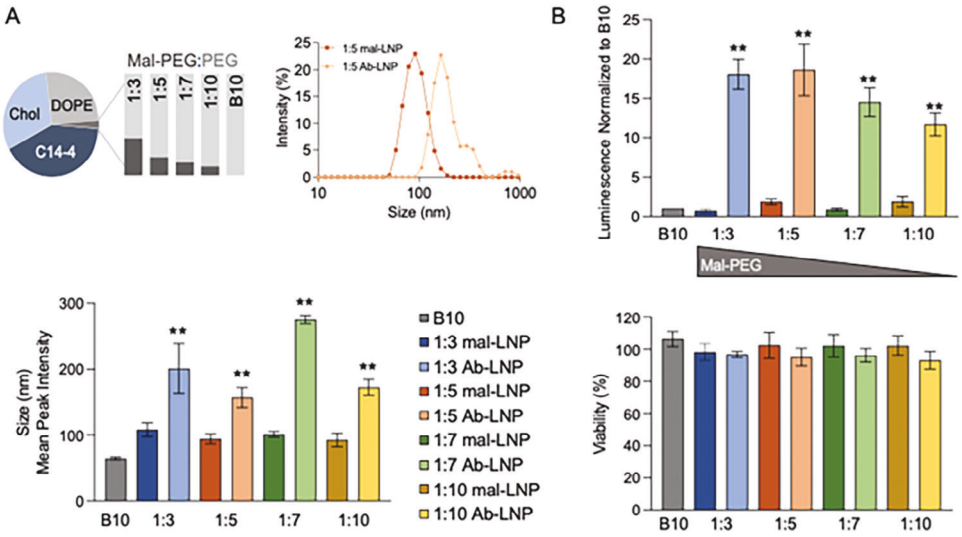

Figure 2. Ab-LNPs show increased size and efficacy over mal-LNPs. A) A library of mal-LNPs were formulated by holding the excipient ratios constant while varying the ratio of mal-PEG:PEG, allowing for varied amounts of anti-CD5 human antibody to bind to the mal-LNP surface. The library was then measured using DLS to observe changes in size before and after conjugation with a representative DLS curve of the 1:5 mal-LNP and Ab-LNP shown and average diameters (mean peak intensity) summarized ($n = 3$, error bars = standard deviation). Statistical analysis included one-way ANOVA with Bonferroni correction, $^{**}p < 0.001$ as compared to B10. B) A screen of the mal-LNP and Ab-LNP library was performed in Jurkat cells (CD5+) at a dose of 50 ng/60 000 cells to measure luciferase-encoding mRNA delivery and cell viability at 24 h ($n = 3$ biological replicates, error bars = standard deviation). Results measuring luminescence were normalized to B10 delivery, and viability was normalized to untreated cells. Statistical analysis included one-way ANOVA with Bonferroni correction, $^{**}p < 0.001$ as compared to B10.

regardless of the mal-PEG to PEG ratio, illustrating the impact of antibody targeting even at lower antibody densities. However, when observing the relative delivery across mal-PEG:PEG ratios, the 1:3 and 1:5 LNP formulations resulted in the highest normalized luminescence while the 1:7 and 1:10 LNP formulations trended toward decreased delivery. This reflects a trend in more antibodies per LNP leading to better cellular uptake, with a plateau in this improvement occurring at 1:5 mPEG:PEG. Thus, as the 1:5 LNP formulation achieved the highest delivery— similar to the 1:3 LNP formulation —while utilizing fewer antibodies, the 1:5 LNP formulation was used throughout the rest of this study.

To further characterize the performance of these Ab-LNPs, both dose response and transfection kinetics were assessed. Over a range of doses, the Ab-LNPs maintained a significant increase in luminescence over both the untargeted B10 and mal-LNP formulations until reaching high doses that also resulted in a significant decrease in cell viability (**Figure 3**A). The increased toxicity of the LNPs was only observed in the Ab-LNP group, with no significant toxicity observed for the B10 or mal-LNP groups. The increased mRNA delivery was also observed at timepoints as early as 4 h at a dose of 50 ng mRNA, indicating that the Ab-LNPs are able to rapidly increase delivery (Figure 3B). Taken together, these results confirmed the increased performance of Ab-LNPs compared to untargeted LNP platforms, warranting further exploration of this Ab-LNP platform.

2.2. Biodistribution of Ab-LNPs Targeting T Cells

While enhanced mRNA delivery with minimal cell toxicity in vitro has implications for improving current ex vivo T cell engineering practices, this investigation sought to explore the potential of these Ab-LNP platforms for in vivo T cell engineering. For this in vivo investigation, the Ab-LNPs incorporated antibodies against mouse CD3 (CD3-LNP), CD5 (CD5-LNP), and CD7 (CD7-LNP) as representative pan-T cell markers. These Ab-LNPs were compared to mal-LNPs at the 1:5 mal-PEG:PEG ratio (mal-B10), B10 LNPs, and DLin-MC3-DMA (MC3) LNPs, a clinical standard that has been utilized in FDA-approved therapies.[30,54] Each of these LNP groups were formulated encapsulating luciferase-encoding mRNA and characterized via DLS to determine their size (**Figure 4**A; Figure S2, Supporting Information). This revealed similar sizes for MC3, B10, and mal-B10 with a size increase from the Ab-LNP groups, as expected. Each of the LNP groups were then administered to mice intravenously at an established well-tolerated dose of 0.6 mg kg^{-1}.[62,63]

After 6 h, biodistribution was assessed using an in vivo imaging system (IVIS) to capture the luminescent signal indicative of functional mRNA delivery to the major organs (Figure 4B; Figure S3, Supporting Information). These images were then used to quantify the luminescent signal from each organ, revealing differences in biodistribution across LNP platforms (Figure 4C). mRNA delivery with the standard MC3 LNP resulted in primarily liver delivery with minimal delivery to both the spleen and lymph nodes (LNs), which is supported by previous investigations exploring MC3 biodistribution.[40,64] The remaining LNPs—all of which contain the C14-4 ionizable lipid—resulted in primarily spleen delivery, with every treatment group achieving enhanced mRNA delivery over the MC3 group. Thus, this ionizable lipid itself may be advantageous for LNPs targeting immune cells.[65–67] Further, of these C14-4 LNPs, the B10 and mal-B10 LNP groups resulted in higher liver delivery compared to MC3 while Ab-LNPs did not result in increased liver transfection, which may suggest

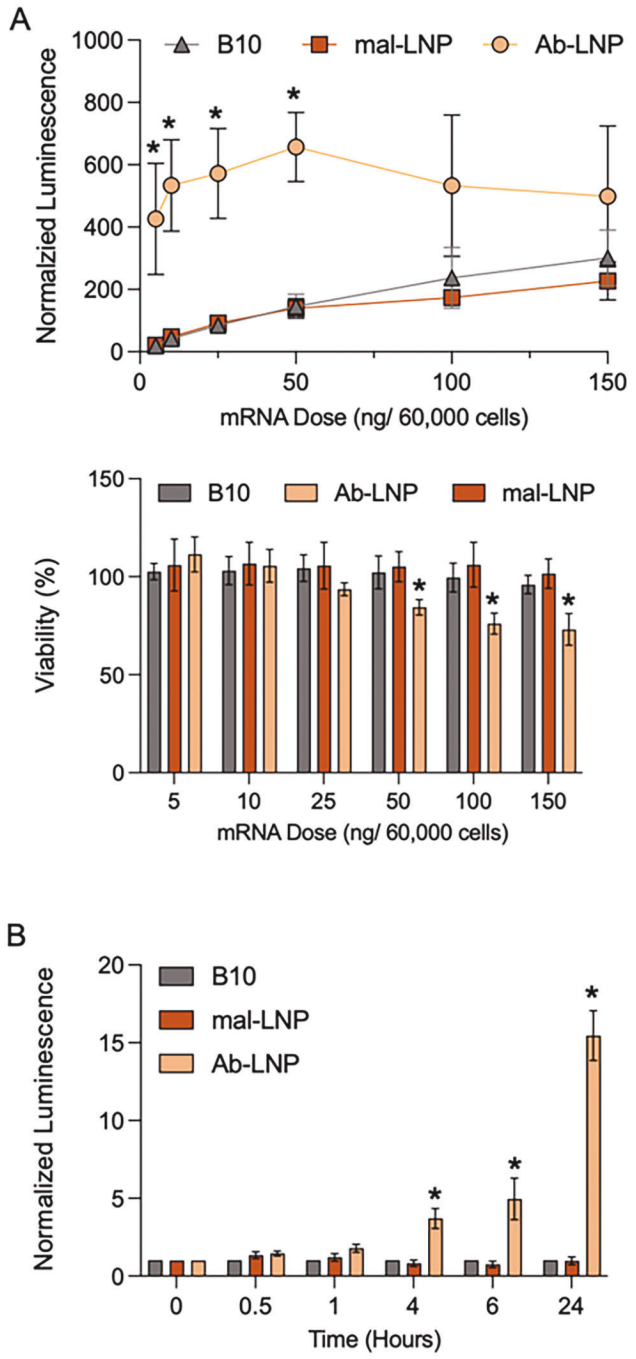

Figure 3. Dose response and kinetics of Jurkat transfection using 1:5 LNPs. A) Luciferase expression and viability of Jurkat cells treated with luciferase-encoding mRNA using 1:5 mal-LNPs and Ab-LNPs for 24 h at a range of mRNA doses, confirming the potency and biocompatibility of the Ab-LNPs ($n = 3$ biological replicates, error bars = standard deviation). Results measuring luminescence were normalized to B10 delivery, and viability was normalized to untreated cells. In both measurements, the results from each treatment group for each dose were compared using a one-way ANOVA with Bonferroni correction, $^{*}p < 0.05$ as compared to B10. B) Luciferase expression of Jurkat cells treated with 1:5 LNPs at 50 ng/ 60 000 cells over a range of 0 to 24 h ($n = 3$ biological replicates, error bars = standard deviation). Statistical analysis included a two-way ANOVA with Bonferroni correction, $^{*}p < 0.05$ as compared to B10 at the same dose.

that the presence of antibodies on the LNP surface aids in bypassing a portion of liver transfection. Luminescence in the LNs across all groups was notably lower than the signal from the liver and spleen, but within this minimal signal there was a significant increase in delivery from the mal-B10, CD3-LNP, and CD7-LNP groups.

As the majority of delivery across all treatment groups occurred in the liver and spleen, the normalized luminescent signals from these organs were then summarized by a comparison of the spleen to liver signal. In this comparison, higher values indicate bias toward splenic delivery over hepatic transfection, which may be beneficial for reaching immune cells. In this comparison, MC3 resulted in the lowest values as it failed to achieve any splenic delivery, and B10 also failed to significantly improve splenic delivery over hepatic. However, the mal-LNP and Ab-LNP groups achieved significantly higher ratios, indicating their increased potential to reach immune cells. From these results, it was concluded that C14-4 LNPs enhanced in vivo mRNA delivery as compared to MC3 with Ab-LNPs showing great promise as the only platforms that did not increase hepatic delivery while also increasing splenic delivery.

To elucidate how this organ-level biodistribution impacts specific immune cell delivery, LNPs were next evaluated for their transfection of immune cells in the blood, spleen, and LNs. Here, LNPs were formulated using GFP-encoding mRNA to allow for cell-level analysis using flow cytometry. 6 h after intravenous administration of 0.6 mg kg^{-1} of mRNA, GFP expression in cells from the blood, spleen, and LNs was measured in a small fraction of the B cell, T cell, and macrophage populations (**Figure 5**A; Figure S4, Supporting Information). The majority of immune cell transfection occurred in the blood for all treatment groups, with varied transfection rates across immune cell types. B10 LNPs demonstrated minimal transfection across all immune cell types, and the mal-B10 LNPs trended toward an increase in macrophage transfection with no significant specificity. Though all three Ab-LNPs had their highest transfection rates in T cells, only CD3-LNPs achieved significant transfection rates in T cells compared to B cells and macrophages, reaching an average of 6.5% GFP positivity in the blood. The same T cell specificity was not observed in the spleen, with the majority of transfection occurring in macrophages. Here, B10 was the only LNP that did not feature increased delivery to macrophages though none of the treatment groups surpassed transfection rates above 1%, indicating minimal delivery to any immune cells overall. Further, no significant immune cell transfection was observed in the LNs, supporting the findings from the luciferase biodistribution. Thus, these results supported the use of Ab-LNPs to achieve immune cell delivery with CD3-LNPs emerging as the most promising platform to transfect circulating T cells.

With CD3-LNPs achieving potent, specific transfection of circulating T cells at 6 h, cell-level biodistribution was next explored at later timepoints. Over 48 h following intravenous administration of either B10 or CD3-LNP groups, GFP expression of T cells, macrophages, and B cells in the blood, spleen, and LNs was assessed (Figure 5B). Across these organs, mRNA delivery was primarily observed in the blood and spleen for both

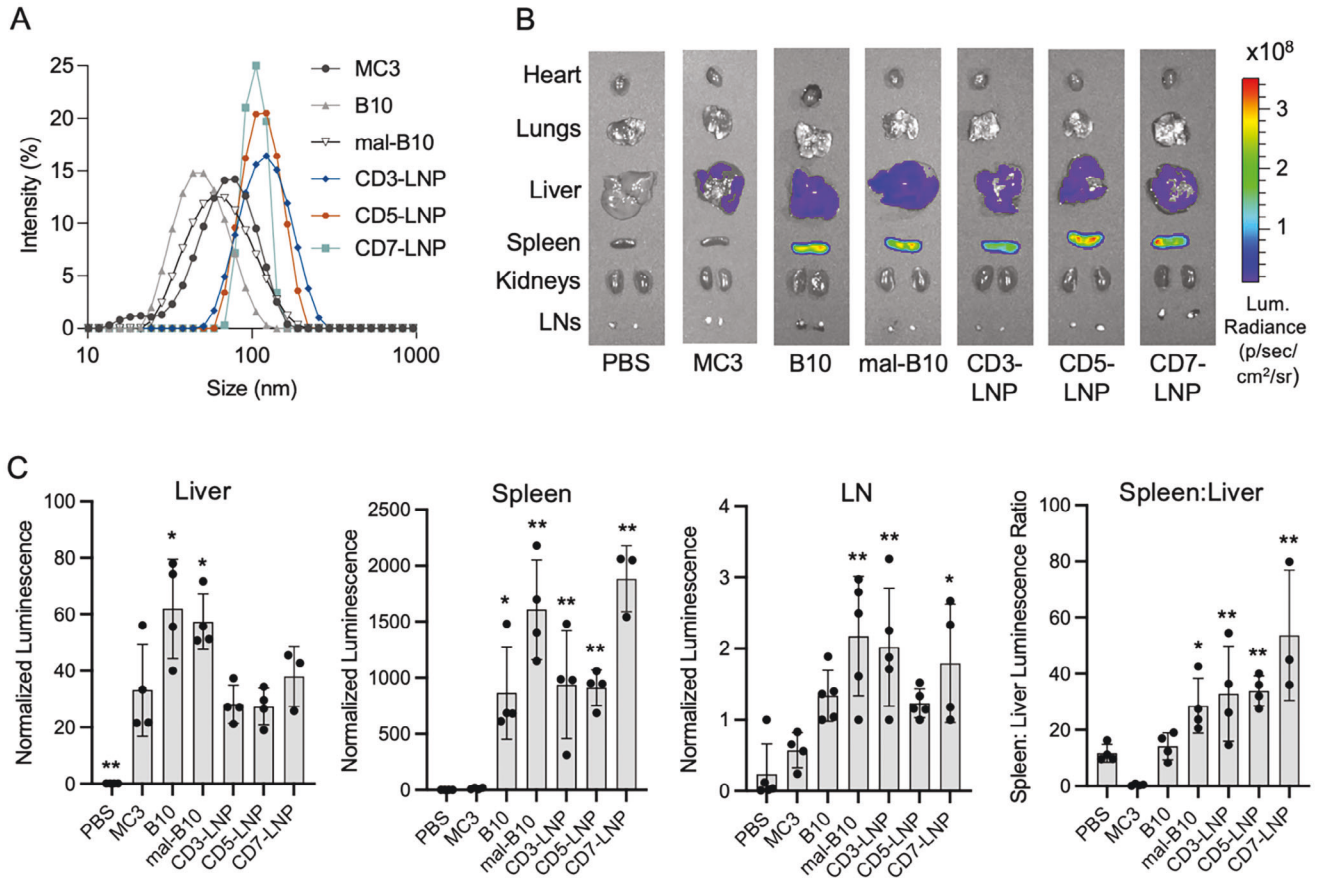

Figure 4. Ab-LNP biodistribution favors spleen delivery compared to standard LNP formulations. A) Representative DLS curves of the LNP treatment groups demonstrating a shift in size following antibody conjugation. B) Representative IVIS images of organs harvested from mice 6 h after intravenous injection of LNPs containing luciferase-encoding mRNA at 0.6 mg kg^{-1}. C) Measurements of luminescence radiance for the liver, spleen, and LNs as regions of interest on the IVIS images normalized to background (n = 4 biological replicates, error bars = standard deviation). The ratio of the normalized luminescence for the spleen and liver of each mouse is also summarized. Statistical analysis included a one-way ANOVA with Dunnett correction, $^{*}p < 0.05$, $^{**}p < 0.001$ as compared to the MC3 treatment group.

LNP groups with only minimal transfection of immune cells in the LNs, even at longer timepoints (Figure S5, Supporting Information). However, the LNP groups achieved transfection in different immune cell populations. In T cells, B10 LNP treatment led to minimal transfection in both the blood and spleen while CD3-LNPs achieved notably potent transfection. In the blood, GFP expression in mice treated with CD3-LNPs decreased over time—an expected outcome of transient mRNA expression, increased motility of T cells following activation, and the potential for T cell depletion associated with CD3 interactions.[32,64,68] In the spleen, GFP expression in T cells significantly increased at 24 h reaching an average of 11% positivity. This is a notable improvement over the ≈4% delivery observed in CD3-targeted MC3 LNPs explored in previous work,[64] possibly due to the observed splenic bias of C14-4 as compared to MC3 in terms of biodistribution. In all, these T cell populations treated with CD3-LNPs featured the highest GFP positivity rates as compared to the other examined immune cell types, supporting the T cell specificity of CD3-LNPs.

Observing the macrophage and B cell populations revealed a few additional trends. In macrophages, an increase in GFP expression in the blood was observed for both B10 and CD3-LNP groups with B10 achieving significantly higher GFP expression than CD3-LNPs at 48 h. Though this represents a small population of macrophages, for CD19-CAR applications, transfection of these cells may induce additional benefit as CAR+ macrophages are also able to eliminate the target B cell population.[69,70] However, in the spleen, both LNP groups demonstrated modest transfection in macrophages with decreased GFP expression over time and no differences between treatment groups. In B cells, there was modest transfection from both LNP groups, but CD3-LNPs had increased delivery compared to B10 in both the blood and spleen. There was a significant increase in B cell transfection in the spleen at 24 h, mirroring the increase observed for T cell transfection at this timepoint though the majority of transfection remained T cell-specific. Further investigations into minimizing B cell interactions may be of interest in future work, though the B cell transfection may be avoided in CD19-CAR applications given the expected depletion in B cells occurring earlier than 24 h. In all, from these results, it was concluded that CD3-LNPs maintained T cell specificity over time with maximum transfection of circulating T cells in the blood occurring at earlier timepoints

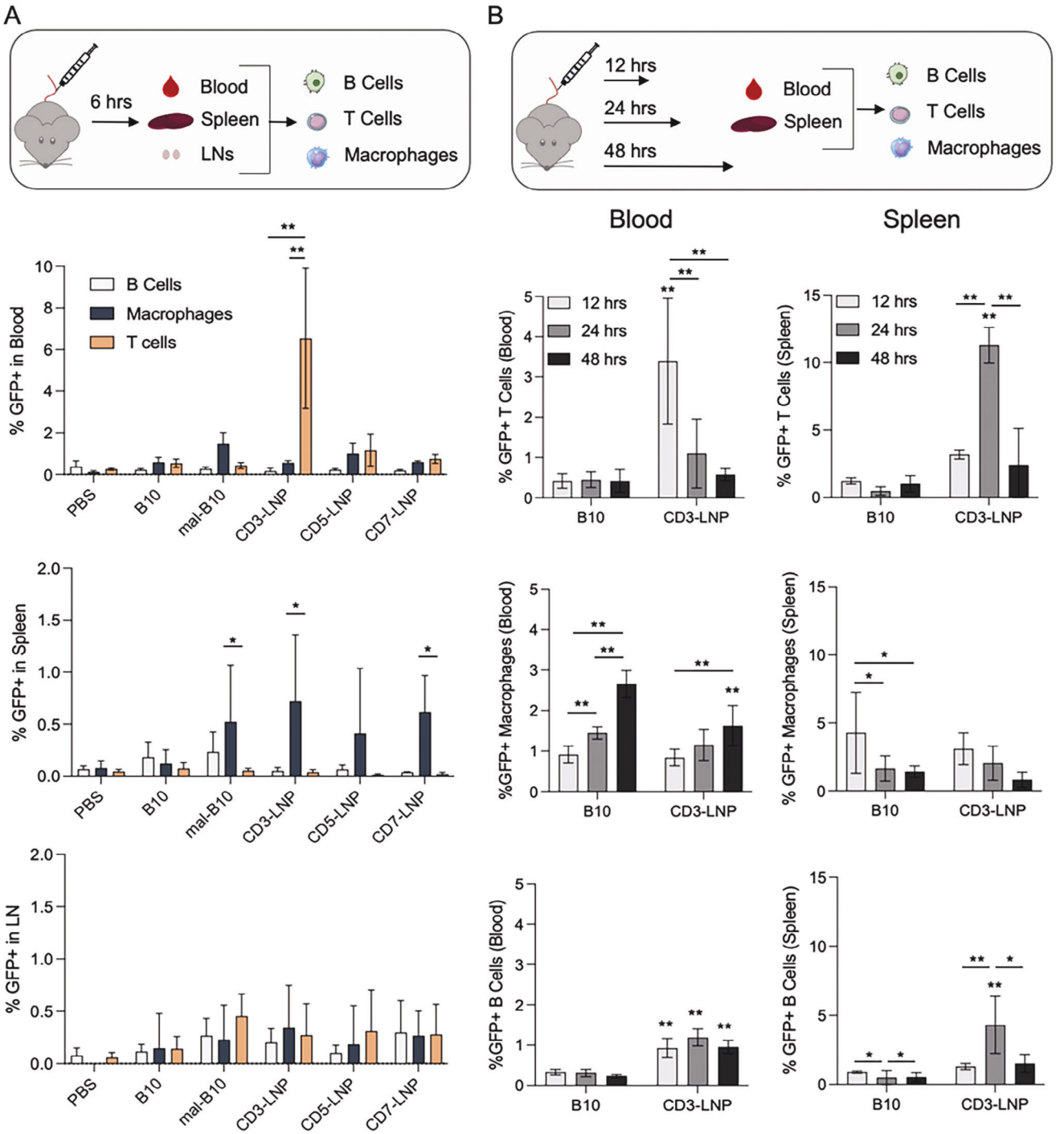

Figure 5. Ab-LNPs demonstrate increased T cell delivery in vivo as compared to untargeted LNPs. A) Transfection rates in the blood, spleen, and lymph nodes of B cells (CD19+), macrophages (CD11b+), and T cells (CD3+) 6 h following 0.6 mg kg^{-1} intravenous injections of LNPs containing GFP-encoding mRNA as measured using flow cytometry ($n = 4$ biological replicates, error bars = standard deviation). Statistical analysis included a two-way ANOVA with Dunnett correction, $^{*}p < 0.05$, $^{**}p < 0.0001$ in marked comparisons. B) Transfection rates in the blood and spleen of T cells, macrophages, and B cells at various timepoints after 0.6 mg kg^{-1} intravenous injections of LNPs containing GFP-encoding mRNA as measured using flow cytometry ($n = 4$ biological replicates, error bars = standard deviation). Statistical analysis included a two-way ANOVA with Tukey correction, $^{*}p < 0.05$, $^{**}p < 0.001$ as compared to B10 at the same timepoint unless noted.

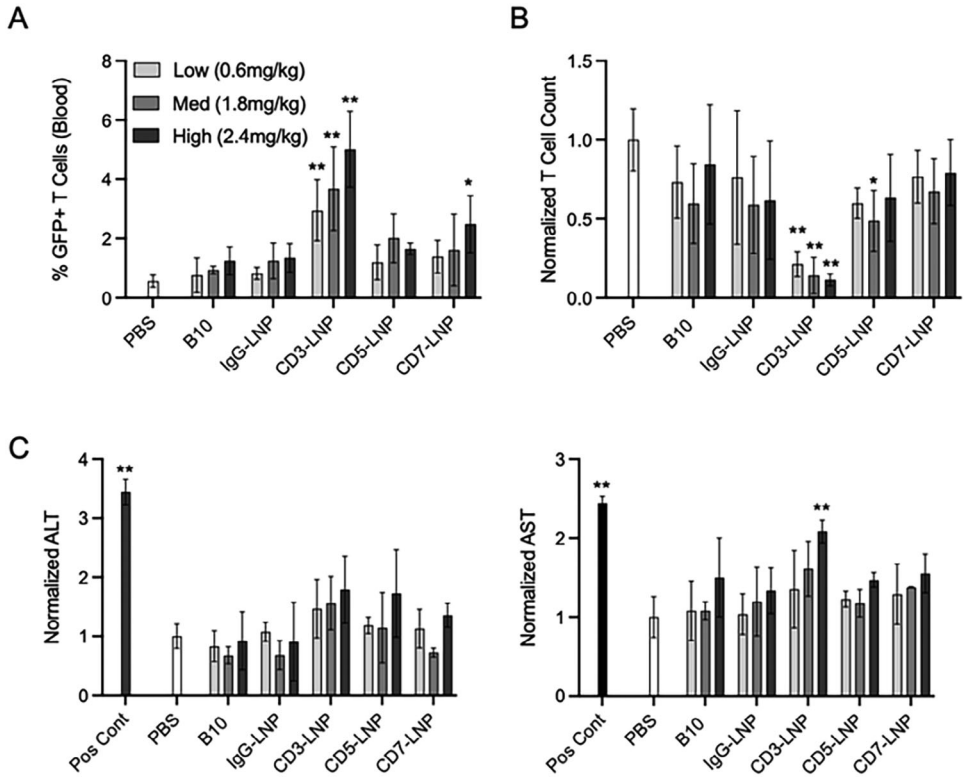

Figure 6. High doses of CD3-LNPs induce T cell population reductions and increased toxicity. A) Transfection rate of T cells in the blood, B) normalized T cell counts, and C) measurements of ALT and AST levels in the serum 24 h after intravenous injection of varied doses of LNPs encapsulating GFP-encoding mRNA ($n = 3$). T cell populations were measured as a percentage of the single cell population, and T cell counts, ALT, and AST were normalized to the PBS treatment group. Statistical analysis included two-way ANOVA with Dunnett correction, $^{*}p < 0.05$, $^{**}p < 0.001$ as compared to PBS.

while B10 led to mostly macrophage transfection with negligible T cell delivery.

2.3. Ab-LNPs Demonstrate Dose-Dependent mRNA Delivery to T Cells In Vivo with Minimal Toxicity

In combination, the biodistribution of Ab-LNPs across organs and immune cell types encouraged the further exploration of these targeted platforms to observe the impact of dose on transfection and toxicity. In these experiments, IgG antibody was conjugated to LNPs to create a non-specific Ab-LNP control group alongside B10 LNPs, and blood was collected 24 h after intravenous injection to assess T cell transfection (**Figure 6**A). Neither of the untargeted controls—B10 and IgG-LNP—yielded significant GFP expression, indicating that specific antibody targeting may be necessary to achieve T cell transfection even at high doses of mRNA. Ab-LNPs exhibited increased GFP expression, though CD5-LNPs did not achieve significant T cell transfection even at the highest dose of 2.4 mg kg^{-1}. CD3-LNPs and CD7-LNPs, however, both induced significant GFP expression at the highest dose with CD3-LNPs demonstrating potent delivery across all doses. This comparison supported CD3-LNPs and CD7-LNPs as promising platforms for T cell targeting.

However, when quantifying the T cell populations in these treatment groups, mice treated with CD3-LNPs had significantly fewer circulating T cells than untreated mice (Figure 6B). This phenomena of T cell depletion following exposure to CD3 antibody—even in the absence of the Fc region—is widely reported as a transient effect induced by CD3-T cell interactions[64,71] though it has not been characterized in many CD3-targeted NP studies. A moderate decrease in T cell count was observed in one dose of the CD5-LNPs, indicating that this depletion of circulating T cells may be induced by other antibodies or T cell interactions as well, but it was not observed for any CD7-LNP doses or any of the untargeted LNPs.

To further investigate the biocompatibility of these LNPs beyond immune cell interactions, the alanine aminotransferase (ALT) and aspartate aminotransferase (AST) serum levels were next evaluated for signs of toxicity. Across doses and treatment groups, there were minimal variations in ALT and AST levels with only the highest dose of CD3-LNPs inducing significant changes (Figure 6C). Thus, moderate doses of all LNP treatments resulted in no signs of liver toxicity, affirming that Ab-LNPs did not generally lead to higher toxicity than untargeted LNPs and allowing for an increased dose to be utilized in subsequent experiments.

2.4. Ab-LNPs Generate Functional CAR T Cells In Vivo

As CD3-LNPs and a high-dose of CD7-LNPs achieved potent delivery to circulating T cells, these Ab-LNPs were next used to deliver a therapeutic cargo—chimeric antigen receptor

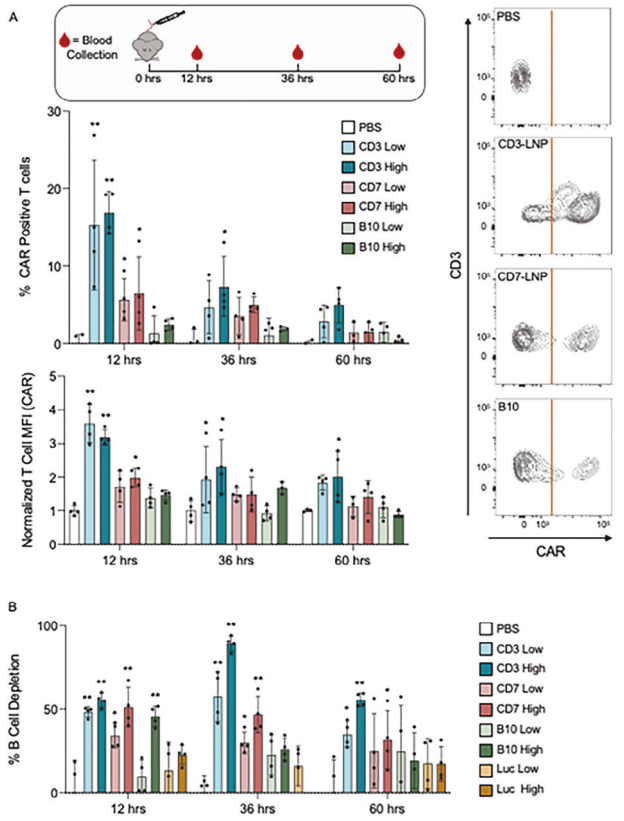

Figure 7. Ab-LNPs generate functional CAR T cells in vivo. A) Transfection rates and mean fluorescent intensity (of the CAR stain) of T cells in the blood at varied timepoints after CAR mRNA delivery at low (0.5 mg kg^{-1}) and high (2 mg kg^{-1}) doses ($n = 4$). Representative contour plots of the CD3+ cell population at 12 h for the PBS, CD3 High, CD7 High, and B10 treatment groups showing CAR positivity gated to the right of the orange line. Statistical analysis included two-way ANOVA with Dunnett correction, $^{*}p < 0.05$, $^{**}p < 0.0001$ as compared to PBS at the same timepoint. B) In these same treatment groups, B cell depletion indicative of CD19-specific CAR T cell activity was calculated as the percent decrease in B cells present in the single cell population as compared to mice treated with PBS. Additional LNP groups containing luciferase-encoding mRNA were included as negative controls for CAR function ($n = 4$). Statistical analysis included a two-way ANOVA with Tukey post hoc correction, $^{*}p < 0.05$, $^{**}p < 0.0001$ as compared to PBS at the same timepoint.

(CAR)-encoding mRNA. The CAR construct utilized in these experiments targeted murine CD19, meaning that functional CAR delivery resulted in the elimination of circulating B cells. Here, CAR mRNA was delivered using B10, CD3-LNPs, or CD7-LNPs at either a low (0.5 mg kg^{-1}) or high (2.0 mg kg^{-1}) dose to evaluate the ability of these LNPs to transfect T cells in a dose-dependent manner, as controlling the concentration of CAR T cells in circulation may be beneficial for mitigating cytokine release and its subsequent side effects.[16,72]

After intravenous administration, circulating T cells were evaluated over 60 h for CAR expression to observe both the relative delivery across LNP platforms and the duration of CAR expression (**Figure 7**A; Figures S6 and S7, Supporting Information). Measurements of CAR expression were accompanied by a comparison of the mean fluorescent intensity (MFI) of the CAR stain within the T cell population, and it should be noted that only a small fraction of the T cell population was observed and analyzed in each sample. At the earliest timepoint of 12 h, both doses of Ab-LNPs led to significant CAR expression with CD3-LNPs reaching 15% and 17% positivity and CD7-LNPs reaching 5% and 6% positivity in circulating T cells at their low and high doses, respectively. The B10 treatment group reached 2% CAR positivity at its higher dose, which was not a significant transfection rate as compared to background from PBS treated mice. Similarly, only the CD3-LNP doses and CD7-LNP high dose achieved increased MFI values in circulating T cells, indicating more potent CAR expression in these groups. At 36 h, CAR positivity and MFI values were lower with only the high dose of CD3-LNPs maintaining a significant percentage of CAR T cells (7%). By 60 h, no groups maintained significant CAR expression, successfully demonstrating the transient nature of the mRNA. However, for the MFI measurements, the high dose of CD3-LNPs continued to show an increase even at 60 h, indicating that the small enduring CAR positive population in this treatment group may maintain potent expression. In all, these findings support the need for targeted LNP approaches to achieve in vivo T cell transfection with therapeutic mRNA cargo, as the B10 LNPs were unable to generate significant CAR T cell populations while the Ab-LNPs demonstrated potent transfection.

To next assess if the observed CAR positivity was indicative of functional CAR T cell generation, B cell elimination was measured. Though the B cells observed in this experiment were not cancerous, the depletion of circulating B cells is indicative of CAR function as it is able to target and eliminate the CD19+ cell population. Here, B10 LNPs containing luciferase mRNA (Luc) were also administered to mice at both the low and high dose to account for any shifts in the circulating B cell population due to the presence of LNPs, and B cell depletion was calculated in comparison to the PBS treated mice (Figure 7B). At the earliest timepoint of 12 h, both doses of the Ab-LNP groups demonstrated a significant decrease in circulating B cells with only the high dose of B10 leading to B cell depletion. At their low and high doses, CD3-LNPs were able to achieve a 49% and 56% decrease in circulating B cells with CD7-LNPs resulting in a 35% and 52% decrease. At the high dose, B10 LNPs achieved a 46% decrease in circulating B cells, but the population recovered by the next timepoint at 36 h. In contrast, at 36 h, the Ab-LNPs led to a more durable B cell depletion with CD3-LNPs decreasing the B cell populations by 58% and 90% for their low and high mRNA doses while the CD7-LNPs maintained more modest decreases of 30% and 47%. By 60 h, the circulating B cell population had recovered in the low dose of CD7-LNPs with the high dose maintaining only a 32% decrease. The CD3-LNPs, however, continued to demonstrate a notable decrease in B cells with a 45% and 56% decrease at the low and high doses, respectively. For these doses and timepoints, there was no observed B cell depletion from the Luc mRNA LNP group, indicating that these decreases were CAR-mRNA dependent. Taken together, this data indicates that the observed CAR expression in T cells corresponded to functional CAR T cell activity in vivo. Both CD3-LNPs and CD7-LNPs achieved significant B cell depletion over 36 h with CD3-LNPs demonstrating a prolonged depletion at 60 h.

In addition to confirming functional CAR T cell production in vivo, serum was collected to observe the impact of LNP treatment and dose on cytokine production. IL-6, TNF-α, and

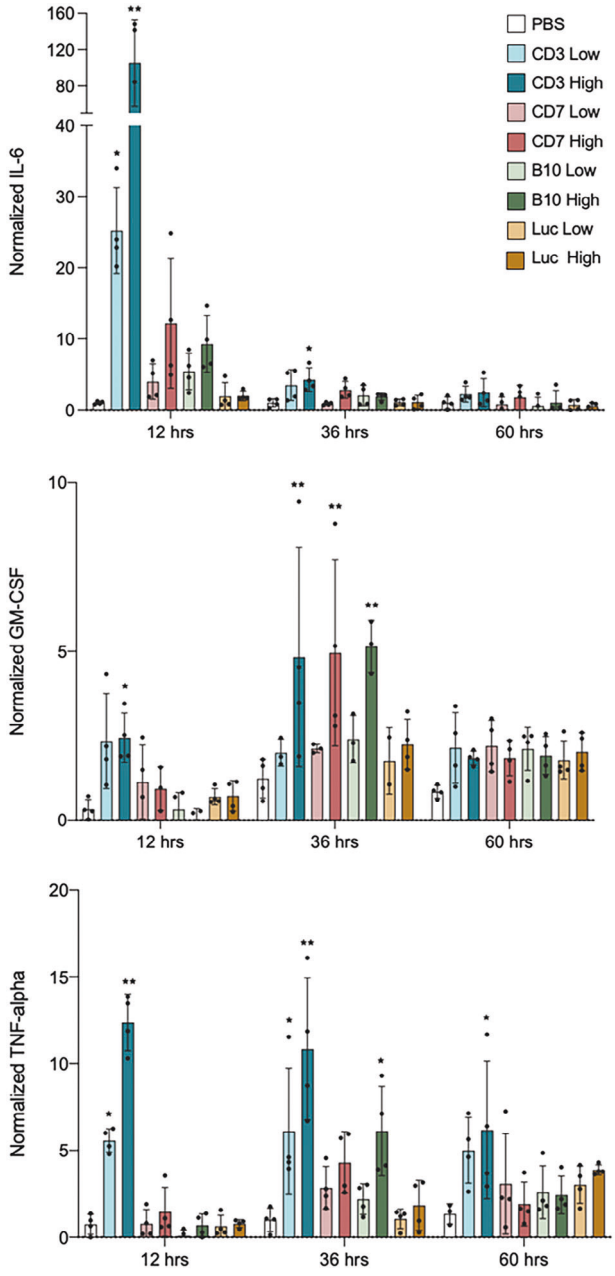

Figure 8. Cytokine levels in the serum of CAR mRNA LNP treated mice. Concentrations of IL-6, GM-CSF, and TNF-alpha in the serum at varied timepoints after CAR mRNA LNP delivery at low (0.5 mg kg^{-1}) and high (2 mg kg^{-1}) doses as normalized to the PBS treated mice ($n = 4$). Statistical analysis included a two-way ANOVA with Dunnett correction, $^{*}p < 0.05$, $^{**}p < 0.0001$.

GM-CSF were assessed as representative cytokines produced during adverse events such as cytokine release syndrome[73,74] (**Figure 8**). At 12 h, CD3-LNPs produced the highest levels of all three cytokines, which is expected as it was the most potent platform for CAR T cell production. Compared to the baseline values of PBS-treated mice, the relative increases in cytokine levels reached here are comparable to the increases observed in low-grade cytokine release in patients receiving traditional CAR T cell therapies.[75] By 36 h, IL-6 serum levels had decreased with only the high dose of CD3-LNPs showing an increase in concentration over PBS. However, serum levels of GM-CSF and TNF-α were still elevated with significant increases in GM-CSF in the high-dose groups of CD3-LNPs, CD7-LNPs, and B10 LNPs and significant increases in TNF-α in both doses of CD3-LNPs as well as the high dose of B10 LNPs. By 60 h, all cytokine levels had returned to normal except for the high-dose CD3-LNP group, which maintained an elevated TNF-α serum concentration. Additionally, across all timepoints, Luc mRNA LNPs did not lead to any elevated cytokine levels, suggesting that the base LNP formulation alone is not inflammatory. Throughout this data, the higher doses of LNPs led to increased serum cytokine levels, supporting the potential for these LNP platforms for CAR T cell production to mitigate cytokine release. Here, the lower dose of CD3-LNPs resulted in lower cytokine serum levels while still producing potent CAR T cells, and the CD7-LNPs led to no significant increases in IL-6 or TNF-α while still achieving high levels of B cell depletion. Further, the transient nature of these increased cytokine levels supports the exploration of repeated dosing to maintain CAR positivity without reaching exceedingly high concentrations of cytokines in the serum. However, in any future work focusing on repeated dosing strategies, the development of antibodies against PEG or any Ab-LNP components should be thoroughly explored to minimize the risk of undesirable effects in the clinic.[76–78] Specifically, future LNP development may explore alternatives to antibody fragments—such as nanobodies—to aid in decreasing anti-drug responses.[79,80] However, in all, these results confirm the ability of these Ab-LNP platforms to achieve potent CAR T cell production in vivo with the potential for tunable cytokine production.

3. Conclusion

In conclusion, this study developed an Ab-LNP platform with extrahepatic tropism for in vivo CAR T cell engineering. Using antibodies against human CD5, Ab-LNPs were screened in Jurkat cells to determine an optimized antibody density by incorporating a range of mal-PEG to PEG ratios into the LNP formulation. These Ab-LNPs were then generated with antibodies against mouse CD3, CD5, or CD7 pan-T cell markers, confirming the versatility of this platform while allowing for a comparison of these T cell targets. Screens of these LNPs in vivo using different reporter cargos revealed the ability of C14-4 LNPs to achieve a higher proportion of spleen transfection over liver transfection than the MC3 clinical standard, with Ab-LNPs demonstrating T cell transfection. Specifically, the CD3-LNPs and CD7-LNPs were able to achieve significant transfection in circulating T cells with specificity over other immune cell types in the observed cell populations. These two Ab-LNP platforms were then formulated with CAR-encoding mRNA and achieved significant CAR positivity in vivo accompanied by potent B cell depletion. Thus, the development of Ab-LNPs—in particular CD3- and CD7-LNPs—was validated as a means to produce functional CAR T cells in vivo. Though future work will be needed to establish the dosing scheme required for robust therapeutic efficacy, evaluate subsequent cytokine release in repeated dosing strategies, and observe larger cell populations to ensure repeatability, Ab-LNPs

demonstrate promise as a platform for CAR T cell engineering as well as other T cell engineering applications.

4. Experimental Section

Ionizable Lipid and mRNA Synthesis: As previously described,[31] S_n2 addition chemistry was used to create the C14-4 ionizable lipid. Briefly, the polyamine core (Enamine Inc., Monmouth Junction, NJ) was combined with an excess of epoxide terminated C14 alkyl chains (epoxytetradecane, Sigma Aldrich, St. Louis, MO) under gentle stirring for 48 h at 80 °C. The crude product was then dried using a Rotovap R-300 (Buchi, New Castle, DE) and resuspended in ethanol to be used for LNP formulation.

mRNA encoding for firefly luciferase (luc), green fluorescent protein (GFP), and anti-murine CD19 (1D3)-specific chimeric antigen receptor (CAR) were all produced from linearized in vitro transcribed (IVT) template plasmids carrying a T7 promoter, 5' and 3' UTR elements, and 101 nucleotide-long poly(A) tail. Cloning and endotoxin-free plasmid preparation service was provided by GenScript (Piscataway, NJ). mRNA was synthesized using the MEGAScript T7 kit (Invitrogen AMB13345) while incorporating m1Ψ−5'-triphosphate (TriLink N-1081) as an alternative to UTP in the IVT reaction. Capping of the IVT mRNAs was performed co-transcriptionally using the trinucleotide cap1 analog, CleanCap (TriLink, San Diego, CA). mRNA was purified by cellulose purification, as previously described.[81] All mRNAs were analyzed by agarose gel electrophoresis and were then stored at −20°C.

Antibody Processing: The antibodies used in this work included the anti-human CD5 (mouse anti-human, UCHT2, ThermoFisher, Waltham, MA, USA), anti-mouse CD3 (hamster anti-mouse, CD3ϵ, BioXCell, Lebanon, NH, USA), anti-mouse CD5 (rat anti-mouse, 53–7.3, Biolegend, San Diego, CA, USA), and anti-mouse CD7 (mouse anti-mouse, 2AE46, Proteintech, Rosemont, IL, USA). The anti-human CD5 antibody was cut using IdeZ, the anti-mouse CD5 was cut using pepsin, and the anti-mouse CD7 antibody was cut using ficin. The anti-mouse CD3 antibody was provided in a F(ab)2 format, and thus, was only reduced.

The IdeZ protease (New England Biolabs, Ipswich, MA, USA) was used as per manufacturer instructions with 1 µL of IdeZ added per 15 ug of antibody for a 90 min reaction at 37°C. Antibodies cut with pepsin (Pierce Fab2 Micro Preparation Kit, ThermoFisher) and ficin (Pierce Mouse IgG1 Fab an Fab2 Micro Preparation Kit, ThermoFisher) utilized microfabrication kits and followed the manufacturer instructions.

The antibody fragments—including the anti-mouse CD3 F(ab)2—were then reduced using dithiothreitol (DTT) via a 30 min incubation at 25°C. The DTT was then removed using centrifugation with a 10 kDa filter (Millipore Sigma, St. Louis, MO, USA), and the antibody product was resuspended in 100 µL PBS.

LNP Formulation and Characterization: LNPs were synthesized, as described previously,[31,82] using a microfluidic device to combine an aqueous phase containing mRNA with an ethanol phase containing the lipid and cholesterol components.[83] The aqueous phase included mRNA in a 10 mM citrate buffer. The ethanol phase contained the ionizable lipid C14-4, 1,2-dioleoyl-sn-glycero-3-phophoe-thanolamine (DOPE) (Avanti Polar Lipids, Alabaster, AL), cholesterol (Sigma, St. Louis, MO), and lipid- anchored polyethylene glycol (PEG) (Avanti Polar Lipids) as well 1,2-distearoyl-sn-glycero-3-phosphoethanolamine (DSPE) -anchored PEG-maleimide (mal-PEG, Avanti Polar Lipids) at a molar ratio of 35 ionizable lipid: 16 DOPE: 46.5 Cholesterol: 2.5 total PEG. The aqueous and ethanol phases were then mixed in the microfluidic device at a 3:1 ratio using Pump 33 DDS syringe pumps (Harvard Apparatus, Holliston, MA). After synthesis, the LNPs were dialyzed against PBS for 2 h before sterilization with 0.22 µm filters and subsequent antibody conjugation.

LNPs were then analyzed in triplicate using dynamic light scattering (DLS) performed on a Zetasizer Nano (Malver Instruments, Malvern, UK) to determine their diameter (z-average) and polydispersity index (PDI). The mRNA concentration of the LNPs was measured via A260 absorbance on an Infinite M Plex plate reader (Tecan, Morrisville, NC).

Ab-LNP Conjugation: Mal-LNPs were combined with cut and reduced antibody fragments at a molar ratio of 1:1 maleimide to antibody fragments, and it was estimated that each antibody that was processed would result in a maximum of 4 antibody fragments. After 1 h at room temperature, the mal-LNPs and antibody were left at 4 °C overnight to complete the reaction. To isolate the Ab-LNPs from the unreacted antibody fragments, including Fc regions, the Ab-LNPs were passed through a column of Sephadex G-75 beads (Millipore Sigma) and collected in ≈200 µL fractions. Any fractions containing mRNA-- as measured via A260/A280 reading on an Infinite M Plex plate reader (Tecan)-- were then pooled as the final Ab-LNP product.

Cell Culture: Jurkat cells (ATCC no. TIB-152), an immortalized human T cell line, were cultured in RPMI-1640 with L-glutamine (ThermoFisher) supplemented with 10% fetal bovine serum and 1% penicillin-streptomycin.

In Vitro Luciferase and Toxicity Assays: Jurkat cells were plated in triplicate at 60 000 cells per 60 µL of supplemented RPMI-1640 media (10% fetal bovine serum, 1% penicillin-streptomycin) in 96-well plates before treatment with LNPs. To determine luciferase mRNA delivery after 24 h—or varying timepoints if noted—the cells were centrifuged at 300 g for 7 min and resuspended in 50 µL of 1X lysis buffer (Promega, Madison, WI) and 100 µL of luciferase assay substrate (Promega). An Infinite M Plex plate reader (Tecan) was then used to measure luminescent signal which was then normalized as described—either to an untreated or control group. To quantify cytotoxicity after 24 h, each well was treated with 60 µL of CellTiter-Glo (Promega). After 10 min of incubation, the luminescence corresponding to ATP production was quantified using an Infinite M Plex plate reader (Tecan), and the signal from each group was normalized to untreated cells.

In Vivo Biodistribution and CAR Delivery: All animal use was conducted in accordance with the Guidelines for Care and Use of Laboratory Animals of University of Pennsylvania and with approval by the Animal Ethics Committee of University of Pennsylvania (protocol 806540). All mice were C57BL/6J, and all treatments were administered via tail vein injections at volumes <200 µL.

For Mice Receiving Luciferase mRNA: 10 min prior to euthanasia, mice were injected intraperitoneally with 150 mg kg^{-1} D-Luciferin, potassium salt (Biotium, Fremont, CA) to visualize the luminescent signal, and luciferase imaging of the harvested organs was then conducted on an in vivo imaging system (IVIS, PerkinElmer, Waltham, MA). Image analysis was completed using the Living Image software (PerkinElmer).

For Mice Receiving GFP or CAR mRNA: Blood samples were collected retro-orbitally into blood collection tubes and centrifuged (8 min, 750 x *g*) to remove serum before repeatedly adding 1 x red blood cell lysis buffer (Invitrogen). When collected, the spleens and lymph nodes were homogenized, and for spleen samples, any red blood cells were lysed using red blood cell lysing buffer. After this processing, the cells from the blood, spleen, and lymph nodes were all resuspended in 0.6% PBSA in a single cell suspension for staining and further analysis.

Both GFP and CAR mRNA treated samples were stained for flow cytometry using the following markers: CD3 (T cells), CD19 (B cells), CD11b (monocytes/ macrophages). Fluorescent stains for these markers included: AF700-CD3 (ThermoFisher), APC-CD3 (ThermoFisher), eFluor450-CD19 (ThermoFisher), PE-eF610-CD11b (ThermoFisher), and PE-CD11b (ThermoFisher). The CAR mRNA treated samples were also stained using a biotinylated mouse CD19 protein (Sino Biological, Wayne, PA, USA) followed by either Streptavidin-AF488 (ThermoFisher) or Streptavidin-FITC (Avantor, Radnor, PA, USA). All of the stains were diluted according to the manufacturer recommendations and used to stain cell samples on ice for 20–30 min before two washes in PBSA. The cells were then analyzed on a BD LSR II Flow Cytometer (BD Biosciences, Macquarie Park, NSW, Australia). Standard gating was performed for doublet exclusion and cell populations were identified as positive for their marker and negative for the remaining cell population stains. For example, T cells were identified as $CD3^+CD19^-CD11b^-$. When observing the depletion of

T cells and B cells, the populations of these specific cells were quantified as the fraction of that cell type within the single cell population.

Toxicity and Cytokine Assays: To first isolate the serum, whole blood was centrifuged for 8 min at 750 x *g*, and the supernatant was collected. This serum was then diluted per manufacturer instructions for the following assays. These assays quantified concentrations of AST, ALT, IL-6, TNF-alpha, and GM-CSF. AST and ALT were quantified using colorimetric assay kits (Cayman Chemicals, Ann Arbor, Michigan, USA) that were performed according to manufacturer recommendations. The IL-6, TNF-alpha, and GM-CSF were quantified using colorimetric Qantikine ELISA kits (bio-techne, R&D systems, Minneapolis, MN, USA) per manufacturer instructions.

Supporting Information

Supporting Information is available from the Wiley Online Library or from the author.

Acknowledgements

M.J.M. acknowledges support from an NIH Director's New Innovator Award (no. DP2TR002776), an NSF CAREER Award (no. CBET-2145491), a Burroughs Wellcome Fund Career Award at the Scientific Interface and the American Cancer Society (no. RSG-22-122-01-ET).

Conflict of Interest

M.M.B. and M.J.M. have filed a patent application on this research. D.W. is named on patents that describe the use of nucleoside-modified mRNA as a platform to deliver therapeutic proteins and vaccines. D.W. and M.G.A. are named on patents describing the use of lipid nanoparticles for nucleic acid delivery. The other authors declare no competing interests.

Data Availability Statement

The data that support the findings of this study are available from the corresponding author upon reasonable request.

Keywords

antibody targeting, CAR T cell, lipid nanoparticle, mRNA

Received: May 25, 2023
Revised: October 16, 2023
Published online:

[1] FDA U.S. Food & Drug Administration. https://www.fda.gov/news-events/press-announcements/fda-approves-first-cell-based-gene-therapy-adult-patients-multiple-myeloma (accessed: March **2021**).
[2] N. Bouchkouj, Y. L. Kasamon, R. A. De Claro, B. George, X. Lin, S. Lee, G. M. Blumenthal, W. Bryan, A. E. Mckee, R. Pazdur, *Clin. Cancer Res.* **2019**, *25*, 1702.
[3] FDA Approves First Cell-Based Gene Therapy For Adult Patients with Relapsed or Refractory MCL, **2020**.
[4] FDA approval brings first gene therapy to the United States, https://www.fda.gov/news-events/press-announcements/fda-approval-rings-first-gene-therapy-united-states, **2020**.
[5] S. L. Maude, N. Frey, P. A. Shaw, R. Aplenc, D. M. Barrett, N. J. Bunin, A. Chew, V. E. Gonzalez, Z. Zheng, S. F. Lacey, Y. D. Mahnke, J. J. Melenhorst, S. R. Rheingold, A. Shen, D. T. Teachey, B. L. Levine, C. H. June, D. L. Porter, S. A. Grupp, *N. Engl. J. Med.* **2014**, *371*, 1507.
[6] Y. Liu, X. Chen, W. Han, Y. Zhang, *Drugs Today* **2017**, *53*, 597.
[7] D. L. Porter, B. L. Levine, M. Kalos, A. Bagg, C. H. June, *N. Engl. J. Med.* **2011**, *365*, 725.
[8] C. E. Brown, D. Alizadeh, R. Starr, L. Weng, J. R. Wagner, A. Naranjo, J. R. Ostberg, M. S. Blanchard, J. Kilpatrick, J. Simpson, A. Kurien, S. J. Priceman, X. Wang, T. L. Harshbarger, M. D'apuzzo, J. A. Ressler, M. C. Jensen, M. E. Barish, M. Chen, J. Portnow, S. J. Forman, B. Badie, *N. Engl. J. Med.* **2016**, *375*, 2561.
[9] J. G. Berdeja, Y. Lin, N. S. Raje, D. S. D. Siegel, N. C. Munshi, M. Liedtke, S. Jagannath, M. V. Maus, A. Turka, L. P. Lam, K. Hege, R. Morgan, M. T. Quigley, J. Kochenderfer, *J. Clin. Oncol.* **2017**, *35*, 3010.
[10] M.-R. Benmebarek, C. Karches, B. Cadilha, S. Lesch, S. Endres, S. Kobold, *Int. J. Mol. Sci.* **2019**, *20*, 1283.
[11] M. Namuduri, R. J. Brentjens, *Expert Rev. Hematol.* **2016**, *9*, 511.
[12] Y. Seow, M. J. Wood, *Mol. Ther.* **2009**, *17*, 767.
[13] D. Putnam, *Nat. Mater.* **2006**, *5*, 439.
[14] N. Pardi, M. J. Hogan, F. W. Porter, D. Weissman, *Nat. Rev. Drug Discovery* **2018**, *17*, 261.
[15] E. Smits, P. Ponsaerts, M. Lenjou, G. Nijs, D. R. Van Bockstaele, Z. N. Berneman, V. F. I. Van Tendeloo, *Leukemia* **2004**, *18*, 1898.
[16] D. M. Barrett, Y. Zhao, X. Liu, S. Jiang, C. Carpenito, M. Kalos, R. G. Carroll, C. H. June, S. A. Grupp, *Hum. Gene Ther.* **2011**, *22*, 1575.
[17] Y. Zhao, E. Moon, C. Carpenito, C. M. Paulos, X. Liu, A. L. Brennan, A. Chew, R. G. Carroll, J. Scholler, B. L. Levine, S. M. Albelda, C. H. June, *Cancer Res.* **2010**, *70*, 9053.
[18] J. B. Foster, N. Choudhari, J. Perazzelli, J. Storm, T. J. Hofmann, P. Jain, P. B. Storm, N. Pardi, D. Weissman, A. J. Waanders, S. A. Grupp, K. Karikó, A. C. Resnick, D. M. Barrett, *Hum. Gene Ther.* **2018**, *30*, 168.
[19] T. S. Rajan, A. Gugliandolo, P. Bramanti, E. Mazzon, *Int. J. Mol. Sci.* **2020**, *21*, 1.
[20] M. A. Islam, E. K. G. Reesor, Y. Xu, H. R. Zope, B. R. Zetter, J. Shi, *Biomater. Sci.* **2015**, *3*, 1519.
[21] A. J. Mukalel, R. S. Riley, R. Zhang, M. J. Mitchell, *Cancer Lett.* **2019**, *458*, 102.
[22] B. R. Olden, Y. Cheng, J. L. Yu, S. H. Pun, *J. Controlled Release* **2018**, *282*, 140.
[23] R. Zhang, M. M. Billingsley, M. J. Mitchell, *J. Controlled Release* **2018**, *292*, 256.
[24] K. J. Kauffman, J. R. Dorkin, J. H. Yang, M. W. Heartlein, F. Derosa, F. F. Mir, O. S. Fenton, D. G. Anderson, *Nano Lett.* **2015**, *15*, 7300.
[25] K. A. Hajj, K. A. Whitehead, *Nat. Rev. Mater.* **2017**, *2*, 17056.
[26] C. J. McKinlay, N. L. Benner, O. A. Haabeth, R. M. Waymouth, P. A. Wender, *Proc. Natl. Acad. Sci. USA* **2018**, *115*, E5859.
[27] M. A. Oberli, A. M. Reichmuth, J. R. Dorkin, M. J. Mitchell, O. S. Fenton, A. Jaklenec, D. G. Anderson, R. Langer, D. Blankschtein, *Nano Lett.* **2017**, *17*, 1326.
[28] L. A. Jackson, E. J. Anderson, N. G. Rouphael, P. C. Roberts, M. Makhene, R. N. Coler, M. P. McCullough, J. D. Chappell, M. R. Denison, L. J. Stevens, A. J. Pruijssers, A. McDermott, B. Flach, N. A. Doria-Rose, K. S. Corbett, K. M. Morabito, S. O'Dell, S. D. Schmidt, P. A. Swanson, M. Padilla, J. R. Mascola, K. M. Neuzil, H. Bennett, W. Sun, E. Peters, M. Makowski, J. Albert, K. Cross, W. Buchanan, R. Pikaart-Tautges, et al., *N. Engl. J. Med.* **2020**, *383*, 1920.
[29] A. B. Vogel, I. Kanevsky, Y. Che, K. A. Swanson, A. Muik, M. Vormehr, L. M. Kranz, K. C. Walzer, S. Hein, A. Güler, J. Loschko, M. S. Maddur, A. Ota-Setlik, K. Tompkins, J. Cole, B. G. Lui, T. Ziegenhals, A. Plaschke, D. Eisel, S. C. Dany, S. Fesser, S. Erbar, F. Bates, D. Schneider, B. Jesionek, B. Sänger, A.-K. Wallisch, Y. Feuchter, H. Junginger, S. A. Krumm, et al., *Nature* **2021**, *592*, 283.
[30] K. Garber, *Nat. Biotechnol.* **2018**, *36*, 777.
[31] M. M. Billingsley, N. Singh, P. Ravikumar, R. Zhang, C. H. June, M. J. Mitchell, *Nano Lett.* **2020**, *20*, 1578.

[32] M. M. Billingsley, A. G. Hamilton, D. Mai, S. K. Patel, K. L. Swingle, N. C. Sheppard, C. H. June, M. J. Mitchell, *Nano Lett.* **2022**, *22*, 533.
[33] X. Wang, I. Rivière, *Mol. Ther. Oncolytics* **2016**, *3*, 16015.
[34] P. Vormittag, R. Gunn, S. Ghorashian, F. S. Veraitch, *Curr. Opin. Biotechnol.* **2018**, *53*, 164.
[35] M. L. Cooper, J. Choi, K. Staser, J. K. Ritchey, J. M. Devenport, K. Eckardt, M. P. Rettig, B. Wang, L. G. Eissenberg, A. Ghobadi, L. N. Gehrs, J. L. Prior, S. Achilefu, C. A. Miller, C. C. Fronick, J. O'neal, F. Gao, D. M. Weinstock, A. Gutierrez, R. S. Fulton, J. F. Dipersio, *Leukemia* **2018**, *32*, 1970.
[36] M. J. Mitchell, M. M. Billingsley, R. M. Haley, M. E. Wechsler, N. A. Peppas, R. Langer, *Nat. Rev. Drug Discovery* **2021**, *20*, 101.
[37] C. Von Roemeling, W. Jiang, C. K. Chan, I. L. Weissman, B. Y. S. Kim, *Trends Biotechnol.* **2017**, *35*, 159.
[38] A. C. Marques, P. J. Costa, S. Velho, M. H. Amaral, *J. Controlled Release* **2020**, *320*, 180.
[39] S. B. Brown, L. Wang, R. R. Jungels, B. Sharma, *Acta Biomater.* **2019**, *101*, 469.
[40] S. Ramishetti, I. Hazan-Halevy, R. Palakuri, S. Chatterjee, S. Naidu Gonna, N. Dammes, I. Freilich, L. K. Shmuel, D. Danino, D. Peer, *Adv. Mater.* **2020**, *32*, 10.
[41] J. Lou, A. Heater, G. Zheng, *Small Struct.* **2021**, *2*, 2100026.
[42] T. T. Smith, S. B. Stephan, H. F. Moffett, L. E. Mcknight, W. Ji, D. Reiman, E. Bonagofski, M. E. Wohlfahrt, S. P. S. Pillai, M. T. Stephan, *Nat. Nanotechnol.* **2017**, *12*, 813.
[43] N. N. Parayath, S. B. Stephan, A. L. Koehne, P. S. Nelson, M. T. Stephan, *Nat. Commun.* **2020**, *11*, 6080.
[44] D. Schmid, C. G. Park, C. A. Hartl, N. Subedi, A. N. Cartwright, R. B. Puerto, Y. Zheng, J. Maiarana, G. J. Freeman, K. W. Wucherpfennig, D. J. Irvine, M. S. Goldberg, *Nat. Commun.* **2017**, *8*, 1747.
[45] J.-E. Zhou, L. Sun, Y. Jia, Z. Wang, T. Luo, J. Tan, X. Fang, H. Zhu, J. Wang, L. Yu, Z. Yan, *J. Controlled Release* **2022**, *350*, 298.
[46] M. D. Mchugh, J. Park, R. Uhrich, W. Gao, D. A. Horwitz, T. M. Fahmy, *Biomaterials* **2015**, *59*, 172.
[47] S. Ramishetti, R. Kedmi, M. Goldsmith, F. Leonard, A. G. Sprague, B. Godin, M. Gozin, P. R. Cullis, D. M. Dykxhoorn, D. Peer, *ACS Nano* **2015**, *9*, 6706.
[48] I. Tombácz, D. Laczkó, H. Shahnawaz, H. Muramatsu, A. Natesan, A. Yadegari, T. E. Papp, M.-G. Alameh, V. Shuvaev, B. L. Mui, Y. K. Tam, V. Muzykantov, N. Pardi, D. Weissman, H. Parhiz, *Mol. Ther.* **2021**, *29*, 3293.
[49] J. Lee, K.-S. Yun, C. S. Choi, S.-H. Shin, H.-S. Ban, T. Rhim, S. K. Lee, K. Y. Lee, *Bioconjug. Chem.* **2012**, *23*, 1174.
[50] J. G. Rurik, I. Tombácz, A. Yadegari, P. O. Méndez Fernández, S. V. Shewale, L. Li, T. Kimura, O. Y. Soliman, T. E. Papp, Y. K. Tam, B. L. Mui, S. M. Albelda, E. Puré, C. H. June, H. Aghajanian, D. Weissman, H. Parhiz, J. A. Epstein, *Science.* **2022**, *375*, 91.
[51] W. Ou, R. K. Thapa, L. Jiang, Z. C. Soe, M. Gautam, J.-H. Chang, J.-H. Jeong, S. K. Ku, H.-G. Choi, C. S. Yong, J. O.h Kim, *J. Controlled Release* **2018**, *281*, 84.
[52] D. Sommermeyer, M. Hudecek, P. L. Kosasih, T. Gogishvili, D. G. Maloney, C. J. Turtle, S. R. Riddell, *Leukemia* **2016**, *30*, 492.
[53] C. J. Turtle, L.-A. Hanafi, C. Berger, T. A. Gooley, S. Cherian, M. Hudecek, D. Sommermeyer, K. Melville, B. Pender, T. M. Budiarto, E. Robinson, N. N. Steevens, C. Chaney, L. Soma, X. Chen, C. Yeung, B. Wood, D. Li, J. Cao, S. Heimfeld, M. C. Jensen, S. R. Riddell, D. G. Maloney, *J. Clin. Invest.* **2016**, *126*, 2123.
[54] S. C. Semple, A. Akinc, J. Chen, A. P. Sandhu, B. L. Mui, C. K. Cho, D. W. Y. Sah, D. Stebbing, E. J. Crosley, E. Yaworski, I. M. Hafez, J. R. Dorkin, J. Qin, K. Lam, K. G. Rajeev, K. F. Wong, L. B. Jeffs, L. Nechev, M. L. Eisenhardt, M. Jayaraman, M. Kazem, M. A. Maier, M. Srinivasulu, M. J. Weinstein, Q. Chen, R. Alvarez, S. A. Barros, S. De, S. K. Klimuk, T. Borland, et al., *Nat. Biotechnol.* **2010**, *28*, 172.
[55] Y. Granot, D. Peer, *Semin. Immunol.* **2017**, *34*, 68.
[56] P. S. Kowalski, A. Rudra, L. Miao, D. G. Anderson, *Mol. Ther.* **2019**, *27*, 710.
[57] I. Mellman, T. Koch, G. Healey, W. Hunziker, V. Lewis, H. Plutner, H. Miettinen, D. Vaux, K. Moore, S. Stuart, *J. Cell Sci.* **1988**, *65*, 45.
[58] S. B. Mkaddem, M. Benhamou, R. C. Monteiro, *Front. Immunol.* **2019**, *10*, 811.
[59] L. C. Fleischer, S. A. Becker, R. E. Ryan, A. Fedanov, C. B. Doering, H. Trent Spencer, *Mol. Ther. Oncolytics* **2020**, *18*, 149.
[60] R. G. Domingues, I. Lago-Baldaia, I. Pereira-Castro, J. M. Fachini, L. Oliveira, D. Drpic, N. Lopes, T. Henriques, J. R. Neilson, A. M. Carmo, A. Moreira, *Eur. J. Immunol.* **2016**, *46*, 1490.
[61] Z. Dai, W. Mu, Y. Zhao, X. Jia, J. Liu, Q. Wei, T. Tan, J. Zhou, *Mol. Ther.* **2021**, *29*, 2707.
[62] X. Hou, T. Zaks, R. Langer, Y. Dong, *Nat. Rev. Mater.* **2021**, *6*, 1078.
[63] K. L. Swingle, H. C. Safford, H. C. Geisler, A. G. Hamilton, R. A. Joseph, *J. Am. Chem. Soc.* **2023**, *145*, 4691.
[64] A. Kheirolomoom, A. J. Kare, E. S. Ingham, R. Paulmurugan, E. R. Robinson, M. Baikoghli, M. Inayathullah, J. W. Seo, J. Wang, B. Z. Fite, B. Wu, S. K. Tumbale, M. N. Raie, R. Holland Cheng, L. Nichols, A. D. Borowsky, K. W. Ferrara, *Biomaterials* **2022**, *281*, 121339.
[65] O. S. Fenton, K. J. Kauffman, J. C. Kaczmarek, R. L. Mcclellan, S. Jhunjhunwala, M. W. Tibbitt, M. D. Zeng, E. A. Appel, J. R. Dorkin, F. F. Mir, J. H. Yang, M. A. Oberli, M. W. Heartlein, F. Derosa, R. Langer, D. G. Anderson, *Adv. Mater.* **2017**, *29*, 1606944.
[66] J. Chen, Z. Ye, C. Huang, M. Qiu, D. Song, Y. Li, Q. Xu, *Proc. Natl. Acad. Sci. USA* **2022**, *119*, 2207841119.
[67] X. Zhao, J. Chen, M. Qiu, Y. Li, Z. Glass, Q. Xu, *Angew. Chem., Int. Ed.* **2020**, *59*, 20083.
[68] M. F. Krummel, F. Bartumeus, A. Gérard, *Nat. Rev. Immunol.* **2016**, *16*, 193.
[69] M. Klichinsky, M. Ruella, O. Shestova, X. M. Lu, A. Best, M. Zeeman, M. Schmierer, K. Gabrusiewicz, N. R. Anderson, N. E. Petty, K. D. Cummins, F. Shen, X. Shan, K. Veliz, K. Blouch, Y. Yashiro-Ohtani, S. S. Kenderian, M. Y. Kim, R. S. O'connor, S. R. Wallace, M. S. Kozlowski, D. M. Marchione, M. Shestov, B. A. Garcia, C. H. June, S. Gill, *Nat. Biotechnol.* **2020**, *38*, 947.
[70] S. Su, A. Lei, X. Wang, H. Lu, S. Wang, Y. Yang, N. Li, Y. Zhang, J. Zhang, *Cells* **2022**, *11*, 1652.
[71] C. Penaranda, Q. Tang, J. A. Bluestone, *J. Immunol.* **2011**, *187*, 2015.
[72] A. Hartsell, *Biol. Blood Marrow Transplant* **2019**, *25*, S336.
[73] J. Gust, R. Ponce, W. C. Liles, G. A. Garden, C. J. Turtle, *Front. Immunol.* **2020**, *11*, 577027.
[74] H. Zhang, X. Lv, Q. Kong, Y. Tan, *Hum. Vaccines Immunother.* **2022**, *18*, 1.
[75] D. T. Teachey, S. F. Lacey, P. A. Shaw, J. J. Melenhorst, S. L. Maude, N. Frey, E. Pequignot, V. E. Gonzalez, F. Chen, J. Finklestein, D. M. Barrett, S. L. Weiss, J. C. Fitzgerald, R. A. Berg, R. Aplenc, C. Callahan, S. R. Rheingold, Z. Zheng, S. Rose-John, J. C. White, F. Nazimuddin, G. Wertheim, B. L. Levine, C. H. June, D. L. Porter, S. A. Grupp, *Cancer Discov.* **2016**, *6*, 664.
[76] T. J. Povsic, M. G. Lawrence, A. M. Lincoff, R. Mehran, C. P. Rusconi, S. L. Zelenkofske, Z. Huang, J. Sailstad, P. W. Armstrong, P. G. Steg, C. Bode, R. C. Becker, J. H. Alexander, N. F. Adkinson, A. I. Levinson, *J. Allergy Clin. Immunol.* **2016**, *138*, 1712.
[77] E. M. J. Van Brummelen, W. Ros, G. Wolbink, J. H. Beijnen, J. H. M. Schellens, *Oncologist* **2016**, *21*, 1260.
[78] M. Estapé Senti, C. A. De Jongh, K. Dijkxhoorn, J. J. F. Verhoef, J. Szebeni, G. Storm, C. E. Hack, R. M. Schiffelers, M. H. Fens, P. Boross, *J. Controlled Release* **2022**, *341*, 475.
[79] C. Ackaert, N. Smiejkowska, C. Xavier, Y. G. J. Sterckx, S. Denies, B. Stijlemans, Y. Elkrim, N. Devoogdt, V. Caveliers, T. Lahoutte, S.

Muyldermans, K. Breckpot, M. Keyaerts, *Front. Immunol.* **2021**, *12*, 578.
[80] Y. Mei, Y. Chen, J. P. Sivaccumar, Z. An, N. Xia, W. Luo, *Front. Pharmacol.* **2022**, *13*, 963978.
[81] M. Baiersdörfer, G. Boros, H. Muramatsu, A. Mahiny, I. Vlatkovic, U. Sahin, K. Karikó, *Mol. Ther. Nucleic Acids* **2019**, *15*, 26.
[82] S. J. Shepherd, C. C. Warzecha, S. Yadavali, R. El-Mayta, M.-G. Alameh, L. Wang, D. Weissman, J. M. Wilson, D. Issadore, M. J. Mitchell, *Nano Lett.* **2021**, *21*, 5671.
[83] D. Chen, K. T. Love, Y. Chen, A. A. Eltoukhy, C. Kastrup, G. Sahay, A. Jeon, Y. Dong, K. A. Whitehead, D. G. Anderson, *J. Am. Chem. Soc.* **2012**, *134*, 6948.